Microchimica Acta (2021) 188: 220
https://doi.org/10.1007/s00604-021-04856-4

ORIGINAL PAPER

Biomimetic recognition strategy for efficient capture and release of circulating tumor cells

Ji Zheng[1] · Dayong Li[1] · Jin Jiao[1] · Chengjie Duan[1] · Youjing Gong[1] · Hai Shi[1] · Zhongyun Wang[2] · Yang Xiang[1]

Received: 23 January 2021 / Accepted: 11 May 2021 / Published online: 2 June 2021

Abstract

Efficient capture and release of circulating tumor cells play an important role in cancer diagnosis, but the limited affinity of monovalent adhesion molecules in existing capture technologies leads to low capture efficiency, and the captured cells are difficult to be separated. Inspired by the phenomenon that the long tentacles of jellyfish contain multiple adhesion domains and can effectively capture moving food, we have constructed a biomimetic recognition strategy to capture and release tumor cells. In details, gold-coated magnetic nanomaterials (Au@Fe_3O_4 NPs) were first prepared and characterized by scanning electron microscopy, UV-vis absorption spectra, and Zeta potential. Then, the DNA primers modified on Au@Fe_3O_4 nanoparticles can be extended to form many radialized DNA products by rolling circle amplification. These long DNA products resemble jellyfish tentacles and contain multivalent aptamers that can be extended into three dimensions to increase the accessibility of target cells, resulting in efficient, simple, rapid, and specific cells capture. The capture efficiencies are no less than 92% in PBS buffer and 77% in blood. Subsequently, DNase I was selected to degrade biomimetic tentacles to release the captured tumor cells with high viability. This release strategy can not only improve cell viability, but also reduce a tedious release process and unnecessary costs. We believe that the proposed method can be expanded for the capture and release of various tumor cells and will inspire the development of circulating tumor cells analysis.

Keywords Gold-coated magnetic nanomaterials · Biomimetic tentacles · Rolling circle amplification · Multivalent aptamer

Introduction

Circulating tumor cells (CTCs) play a crucial role in tumor metastasis. They are the cancer cells that shed from the primary or metastatic site of the tumor and enter the circulatory system due to spontaneous or objective surgery [1–3]. Most CTCs have a limited half-life and undergo apoptosis during circulation, but a few can survive and metastasize to distant organs, causing metastasis-related death [4]. Capturing these CTCs can contribute to downstream molecular research, which can insight into the mechanisms of tumorigenesis and development and conduct personalized anti-tumor therapy [5, 6]. However, the inherent rarity, vulnerability and heterogeneity of CTCs pose significant technical challenges for their capture and isolation in biological fluids.

Currently, a variety of techniques have been developed for CTCs isolation, such as physical sorting-based cell-free marker assays [7, 8] and affinity-based CellSearch capture techniques [9, 10]. However, limited affinity often leads to inefficient cells capture and difficult isolation of the captured cells. Besides, long separation time and complex operation often lead to cells viability loss and cells damage or fragmentation, which are not conducive to the downstream analysis. Therefore, there is an ever-increasing need of non-destructive and scalable methods for the sort and isolation of CTCs. In recent years, some methods based on nucleic acid amplification [11, 12], multiple recognition elements [13] and

This article is part of the Topical Collection on *Nanomaterials for biomedical imaging and targeting*

✉ Hai Shi
shihai1989@yeah.net

✉ Zhongyun Wang
zywang1970@126.com

✉ Yang Xiang
xiangy@nju.edu.cn

[1] State Key Laboratory of Pharmaceutical Biotechnology, School of Life Sciences, Nanjing University, Nanjing 210023, People's Republic of China

[2] Department of Anesthesiology, The First Affiliated Hospital of Nanjing Medical University, Nanjing 210029, People's Republic of China

DNA assembly [14] have been developed to improve target capture efficiency, recognition specificity, and non-destructive separation. Among them, DNA has been widely used due to its high programmability and unique interaction on the bio-nano interface [15–17].

To satisfy the mentioned demands for disease analysis, nanocomposites have been widely studied because of their functional diversity [18, 19]. Among them, Au@Fe_3O_4 NPs are favored because they not only retain the superparamagnetic property of iron oxides for magnetic separation, but also have the chemical stability and biocompatibility of gold [20–22]. In this work, inspired by the long tentacles of jellyfish that can effectively capture moving food particles in fluids, we have constructed a biomimetic strategy to capture and release tumor cells in body fluid (Scheme 1). Specifically, P1 DNA primers modified on Au@Fe_3O_4 NPs can be extended to form many radialized DNA products by rolling circle amplification (RCA). These long DNA products resemble jellyfish tentacles and contain multiple aptamers, which can be extended to three-dimensional space to capture target cells through multivalent aptamers, thus achieving efficient, rapid, and specific cells capture. Subsequently, the captured CTCs can be effectively released by simple DNase I treatment with little influence on cells activity.

Experimental section

Materials and reagents

Gold (III) chloride trihydrate ($HAuCl_4 \cdot 3H_2O$), tris(2-carboxyethyl)phosphine hydrochloride (TCEP), sodium borohydride ($NaBH_4$), iron(III) chloride hexahydrate ($FeCl_3 \cdot 6H_2O$), ethylene glycol, and sodium acetate (NaAc) were purchased from Sigma-Aldrich (http://www.sigmaaldrich.com/). Deoxynucleotide set (dNTPs) and cell culture medium (Dulbecco's modified eagle's medium, DMEM) were purchased from ThermoFisher Scientific (Shanghai, China, http://www.thermofisher.com/). Rapid DNA ligation kit and calcein AM were obtained from Beyotime Biotechnology. Deoxyribonuclease I (DNase I) was obtained from New England BioLabs (https://international.neb.com/). Dulbecco's PBS (DPBS, pH 7.2 ~ 7.4), phosphate buffered saline (PBS, pH 7.4), phi29 DNA polymerase and the corresponding buffer were purchased from Shanghai Sangon Biotechnology Co., Ltd. (Shanghai, China, http://www.sangon.com/). Whole-blood samples were obtained in healthy donors from Gaochun People's Hospital. Other chemical regents were analytical grade and used without further purification. All solutions were prepared with deionized water purified with a Millipore filtration system (18.2 MΩ cm). All oligonucleotides used in this work were synthesized and purified by Shanghai Generay Biotech Co., Ltd. (Shanghai, China, http:// http://www.generay.com.cn/). The sequences of the DNA oligonucleotides are listed in Table S1.

Preparation of Fe_3O_4 NPs and Au@Fe_3O_4 NPs

Fe_3O_4 nanoparticles (Fe_3O_4 NPs) and Au@Fe_3O_4 nanoparticles (Au@Fe_3O_4 NPs) were synthesized according to the previously reported procedure with a slight modification [23]. More details are available in the supporting information.

Rolling circle amplification reaction on Au@Fe_3O_4 NPs

The RCA reaction was carried out by the method reported in literatures [24–26] with slight modification. It includes two steps: preparation of circular DNA template and final RCA

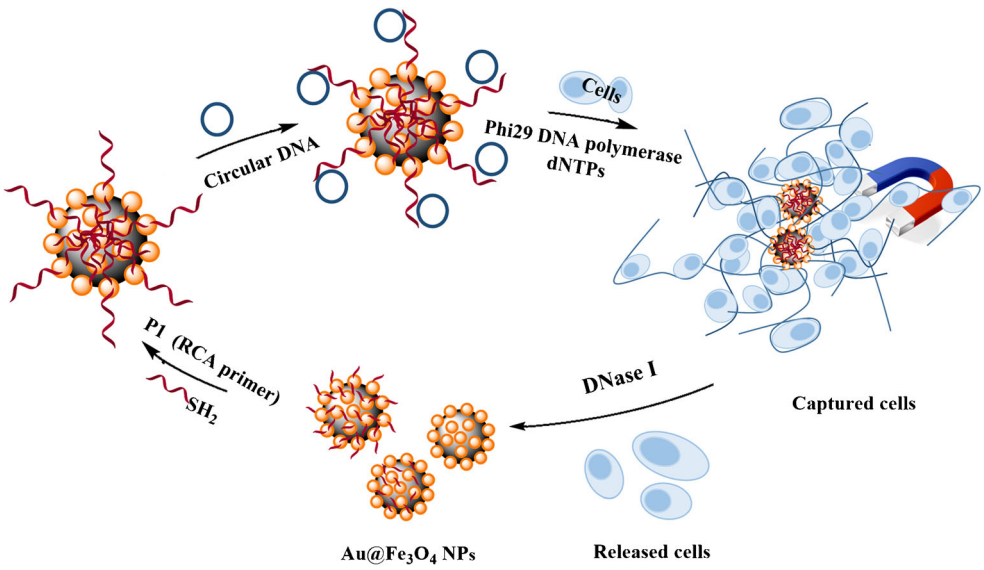

Scheme 1 Schematic illustration of capture and release of tumor cells based on biomimetic recognition strategy

reaction with circular DNA. More details are available in the supporting information.

Cells capture and imaging

HeLa cells (cervical cancer cell line) were cultured in DMEM supplemented with 10% FBS (Gibco, Invitrogen) in a humidified incubator (Thermo 3111) at 37 °C containing 5% CO_2. Cells were collected and counted with an automated cell counter (Invitrogen Countess) for the following experiments.

To evaluate the performance of the method, different numbers of HeLa cells as artificial CTCs were added to PBS buffer (pH 7.4) and diluted samples to explore the capture efficiency. Au@Fe_3O_4 NPs-RCA (4.0×10^6 particles mL^{-1}) were incubated with HeLa cells, HepG2 cells and normal blood cells at 37 °C for 30 min to explore the selectivity.

MTT assay

HeLa cells were first seeded into a 96-well plate at 100 μL/well (1×10^4 cells) according to the instructions. After incubation overnight, the original medium was removed, and different reagents at appropriate concentrations were added to the wells and incubated at 37 °C for 30 min. Subsequently, 50 μL 1 × MTT reagent was added to the wells and incubated at 37 °C for 4 h to reduce MTT to formazan. After the supernatant was removed, 150 μL DMSO was added to each well to dissolve formazan, and the solution was shaken with a plate shaker. The optical signal of each well was detected with a microplate reader at the wavelength of 490 nm.

Cell release and culture

The captured tumor cells were separated with a magnet, added with DNase I (0.5 U μL^{-1}), reacted at 37 °C for 20 min, washed with PBS (pH 7.4) for 3 times, and then stained with calcein AM solution (2 μM) for 40 min. The cells were washed with PBS and cultured in DMEM medium containing 20% fetal bovine serum and 1% penicillin-streptomycin. After culturing for a certain time, the cells were observed under a microscope.

Results and discussion

Characterization of Au@Fe_3O_4 NPs

The morphology of Fe_3O_4 NPs and Au@Fe_3O_4 NPs were characterized by scanning electron microscopy (SEM). Figure 1a shows that the prepared Fe_3O_4 NPs are spherical with an average particle size of about 140 nm. Figure 1b shows that after in situ reduction of the gold (III) chloride trihydrate, there are many small particles attached to the Fe_3O_4 NPs to form Au@Fe_3O_4 NPs. Next, we have explored the as-prepared nanocomposites through UV-vis absorption spectra. Figure 1c, d shows that the color of the Fe_3O_4 NPs solution is brown, and its corresponding UV-vis absorption peak is weak. While the Au@Fe_3O_4 NPs solution is purple black and has a significant UV-vis absorption peak at 560 nm, which attributed to the attachment of AuNPs on surface, and an obvious Au absorption peak can be seen in the energy dispersive spectrometer (EDS) of Fig. 1e, which further proves the successful preparation of Au@Fe_3O_4 NPs.

Preparation of DNA functionalized Au@Fe_3O_4 NPs

The coupling of thiolated P1 DNA to Au@Fe_3O_4 NPs is a key step in designing this biomimetic strategy, and the results were explored by Zeta potential. The Zeta potential of Fig. 2a shows that the electronegativity of the Au@Fe_3O_4-P1 DNA (-56.8 ± 1.8 mV) is stronger than that of the Au@Fe_3O_4 NPs (−24 mV), indicating that the P1 DNA is successfully modified on the Au@Fe_3O_4 NPs surface.

The UV-vis absorption spectrum in Fig. 2b shows that Au@Fe_3O_4-P1 DNA has an obvious ultraviolet absorption peak at 320 nm compared with Au@Fe_3O_4 NPs, and the absorption peak is blue-shifted to some extent. Furthermore, the UV-vis peak of Au@Fe_3O_4-RCA shows a further blue-shifted owing to the loading of a large number of RCA reaction products. It is clear that the thioated P1 DNA is successfully modified on the Au@Fe_3O_4 NPs by covalent binding and further triggers the subsequent RCA reaction on Au@Fe_3O_4 NPs. Besides, the necessity of each element in the solution for the RCA reaction was verified by gel electrophoresis. Figure S1 shows that the RCA reaction could only be initiated when the P1 DNA, circular DNA and phi29 DNA polymerase exist simultaneously (lane 5–8). Meanwhile, we have noticed that the RCA products increased with the extension of amplification time and reached a plateau in 30 min (lane 7). So, 30 min is taken as the optimized reaction time.

Cell capture

To evaluate the feasibility and capture performance of the biomimetic recognition strategy, we have observed the state of cells before and after capture. The results of Fig. S2 show that the method has good feasibility, and Fig. 3 confirms its good performance. In details, Fig. 3a–c show that cells are well dispersed before the addition of Au@Fe_3O_4-RCA products. While Fig. 3d–f show that after the addition of the Au@Fe_3O_4-RCA products, cells are in a highly aggregated state, and the bright field of Fig. 3d shows that there are distinct black spots around the aggregated cells. On the one hand, the aggregation of cells may be attributed to the cross-winding of DNA long-chain products produced in the RCA process.

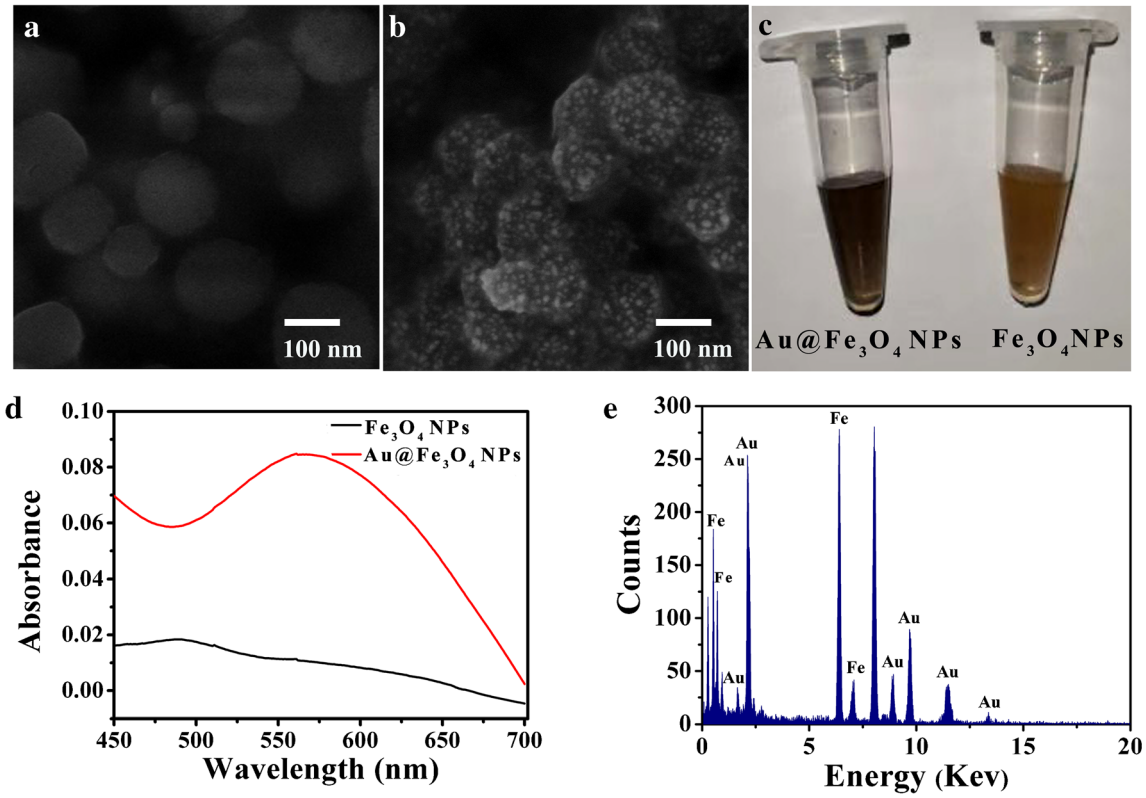

Fig. 1 **a** SEM images of Fe_3O_4 NPs. **b** SEM images of Au@Fe_3O_4 NPs. **c** Color diagrams of Au@Fe_3O_4 NPs solution and Fe_3O_4 NPs solution. **d** Ultraviolet-visible absorption spectra of Au@Fe_3O_4 NPs and Fe_3O_4 NPs. **e** EDS spectral analysis of Au@Fe_3O_4 NPs

The long-chain products contain multiple repetitive nucleic acid aptamers (AS1411), which can bind to nucleolin proteins on the cell membrane through multivalent synergy to trap and cluster the cells around the nanoparticles. On the other hand, as a result of the magnetic field applied during the magnetic separation process, the Au@Fe_3O_4 NPs loaded with RCA products can rapidly gather together, making the captured cells highly aggregated. The larger or smaller black spots around the cells are different aggregation states of Au@Fe_3O_4 NPs which resulted from the magnetic separation as well. In spite of the subsequent washing and resuspension processes, Au@Fe_3O_4 NPs loaded with cells and RCA products are difficult to disperse uniformly in a short time, causing the uneven size of the Au@Fe_3O_4 NPs. To further explore the capture performance of this method, we incubated Au@Fe_3O_4-RCA with different amounts of HeLa cells in PBS buffer and blood samples, respectively. Figure 3g shows excellent performance for cancer cells capture in complex samples and Fig. S3 further demonstrate the good selectivity of this method. In conclusion, the biomimetic tentacles on

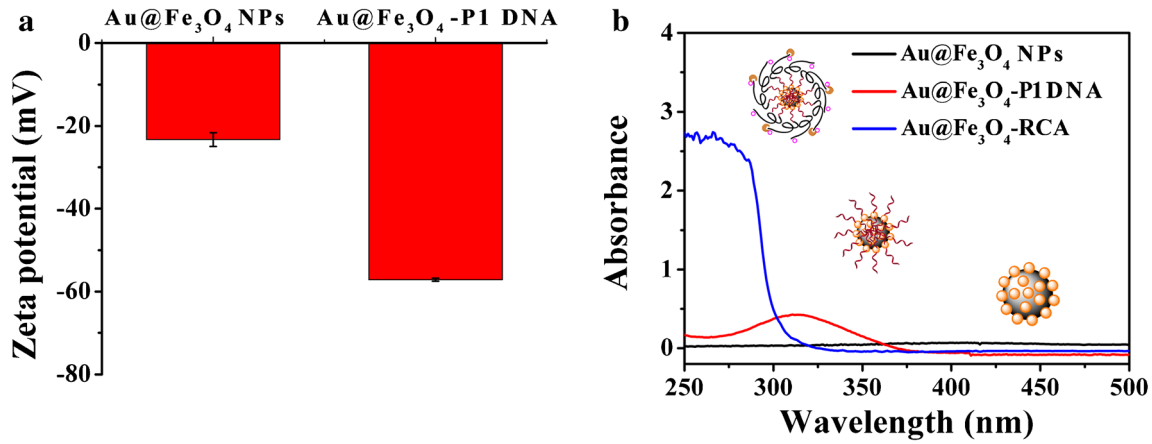

Fig. 2 **a** Zeta potential diagram of Au@Fe_3O_4 NPs and Au@Fe_3O_4-P1 DNA. **b** UV-Vis spectra of Au@Fe_3O_4 NPs, Au@Fe_3O_4-P1 DNA, and Au@Fe_3O_4-RCA. Error bars are the standard deviation of three independent replicates

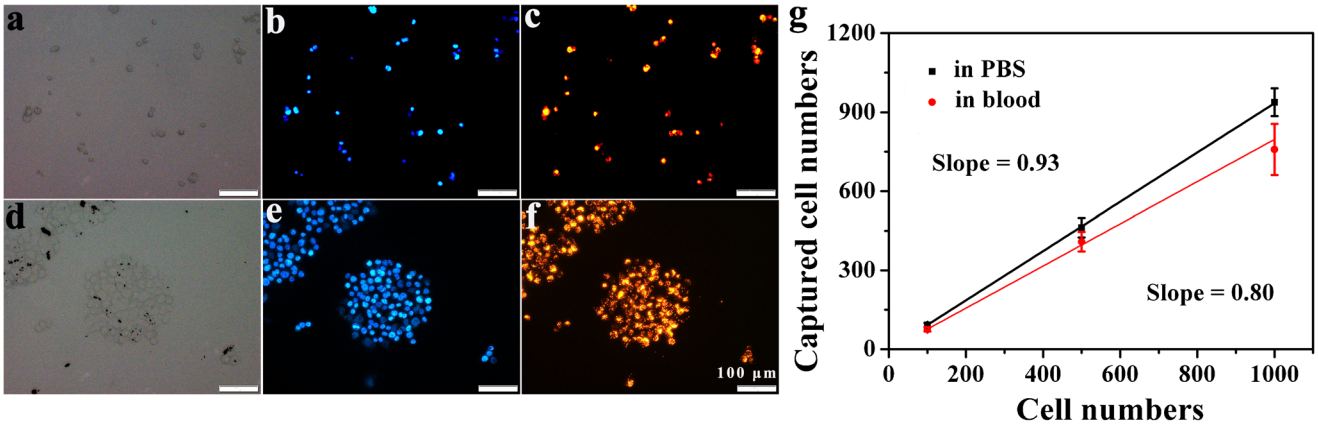

Fig. 3 Bright-field and fluorescence images of cells before and after capture by Au@Fe_3O_4 NPs-RCA products. **a** Bright field of cells before capturing. **b** Hoechst 33342 for nucleus (blue). **c** Cell membrane stain with DiI dye (DiI, orange). **d** Bright field of cells after capturing, the black spots around the cells are Au@Fe_3O_4 NPs. **e** Hoechst 33342 for nucleus (blue). **f** Cell membrane stain with DiI dye (DiI, orange), scale 100 μm. **g** Confirming the capture ability of Au@Fe_3O_4-RCA products to HeLa cells. Error bars represent the standard deviation of three experiments

Au@Fe_3O_4 NPs can capture target cells through multivalent aptamers.

Cell release and post-release activity study

Multidimensional analysis of CTCs can provide more specific and comprehensive disease information, which requires manipulation on live tumor cells [27, 28]. Considering that the construction of the biomimetic strategy is based on the multivalent recognition function of DNA aptamers, the rapid and non-destructive release of captured cells can be achieved through simple DNase I treatment. Figure S4a simulates the cell state before and after release, and Fig. S4b shows the gel electrophoresis pattern of RCA products before and after the addition of DNase I, which indicates that the biomimetic tentacle around the cells can be effectively degraded by DNase I (0.5 U μL^{-1}) within 20 min at 37 °C, thus achieving the release of the target cells. To demonstrate the effectiveness of the capture strategy and the mildness of the release method, we observed the morphological images of captured cells and the fluorescence images of some released cells. Figure 4a, c shows that the cells are highly aggregated near the black Au@Fe_3O_4 NPs, indicating that the prepared Au@Fe_3O_4 NPs with bionic tentacles can capture a large number of cells, and the capture efficiency is positively correlated with the number of cells added. However, some DNase I-treated cells were observed by fluorescence microscope. Figure 4b, d shows that the cells are in a good monodisperse state with good viability. Figure S5 further shows the method has a high release efficiency. Moreover, the cytotoxicity of the materials to cells was evaluated by MTT assay and Fig. 4e shows that cells incubated with materials still retain high viability. These

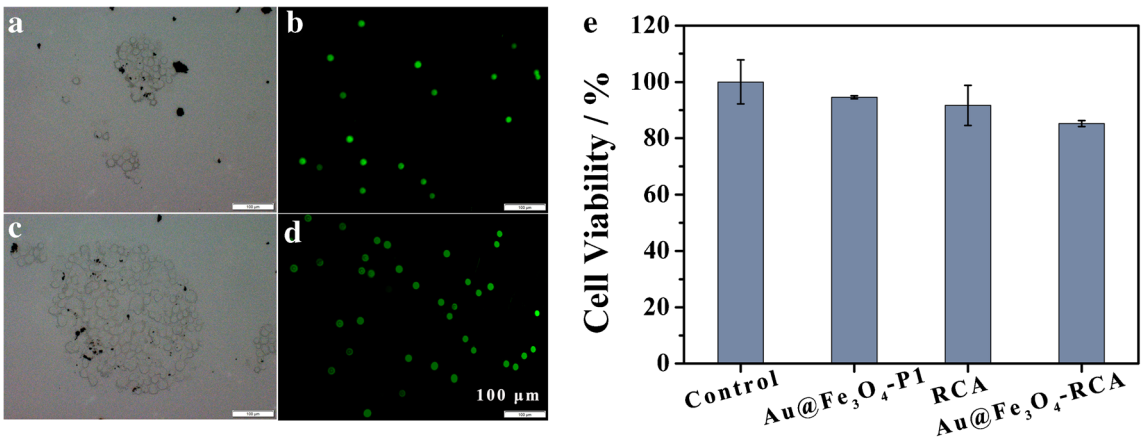

Fig. 4 Morphological images of HeLa cells before capture and fluorescence images after release. **a** Bright field images of 5×10^2 cells mL^{-1}. **b** Fluorescent images of some cells released from **a**. **c** Bright field images of 5×10^4 cells mL^{-1}. **d** Fluorescent images of some cells released from **c**. Cells were stained with 2 μM calcein AM for fluorescence imaging, scale 100 μm. **e** Cell viability analysis of HeLa cells with Au@Fe_3O_4-P1 DNA, RCA products and Au@Fe_3O_4-RCA products. Error bars represent the standard deviation of three experiments

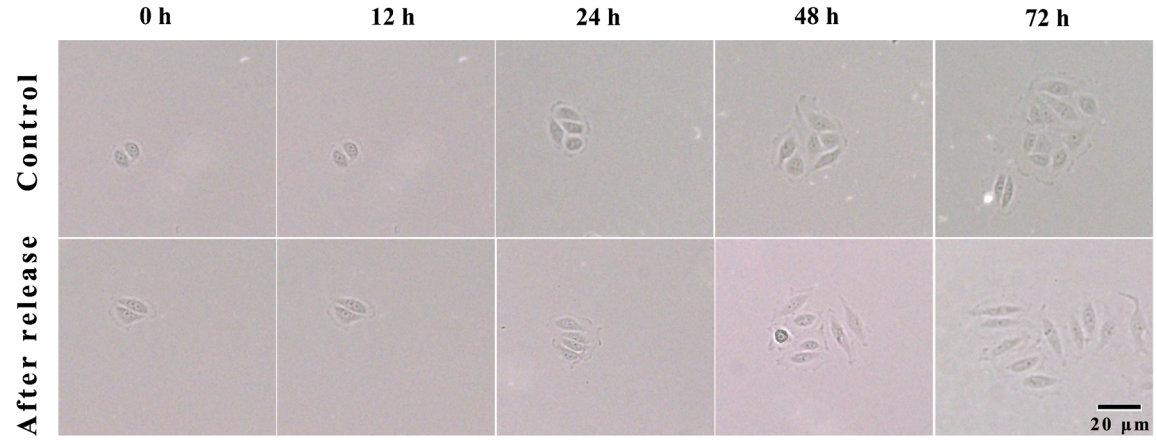

Fig. 5 Morphological observation of proliferation of normal cultured cells and released cells, scale 20 μm

results confirm the feasibility of the capture strategy and the mildness of the release method, both of which are very important for the subsequent multidimensional analysis of CTCs. Finally, we compared performance of our method with existing platforms. Table S2 shows that our method is more efficient for capture and release cells with simple operation [9, 29–32].

Exploration of cell proliferation ability after release

We should not only focus on the effectiveness of the capture strategy, but also on the cells proliferation ability after release. By performing parallel experiments with untreated cells as a control, we assessed the proliferative capacity of the released cells. As can be seen from Fig. 5 and Fig. S6, the division and proliferation of the released cells continued over time, and there was no significant difference on the proliferation ability between the released and normal cultured cells.

Conclusions

In this work, we have developed a biomimetic recognition strategy to capture and release tumor cells. In this method, the multivalent recognition of bionic tentacles can cooperate with the swing of long-chain tentacles to improve the capture performance. The capture efficiency was not less than 92% and 77% in PBS buffer and blood, respectively. The release efficiency is higher than 93%, and the released cells still maintained high viability for further study. Besides, the modular design endows the biomimetic method with universal function. However, the aptamer used in the work are specific to nucleolin and the aptamer for other specific biomarkers may not available. Nevertheless, with the constant screening of aptamers, the analysis of more kinds of tumor cells can be expanded. Therefore, we believe that this biomimetic recognition method has a broad application prospect in biosensing and cancer diagnosis.

Supplementary Information The online version contains supplementary material available at https://doi.org/10.1007/s00604-021-04856-4.

Acknowledgments This work was supported by the National Natural Science Foundation of China (Grant Nos. 81672570 and 81370926 to Yang Xiang).

Declarations

Conflict of interest The authors declare that they have no competing interests.

References

1. Riggi N, Aguet M, Stamenkovic I (2018) Cancer metastasis: a reappraisal of its underlying mechanisms and their relevance to treatment. Annu Rev Pathol 13:117–140
2. Allard WJ, Matera J, Miller MC, Repollet M, Connelly MC, Rao C, Tibbe AGJ, Uhr JW, Terstappen LWMM (2004) Tumor cells circulate in the peripheral blood of all major carcinomas but not in healthy subjects or patients with nonmalignant diseases. Clin Cancer Res 10(20):6897–6904
3. Aceto N, Bardia A, Miyamoto DT, Donaldson MC, Wittner BS, Spencer JA, Yu M, Pely A, Engstrom A, Zhu HL, Brannigan BW, Kapur R, Stott SL, Shioda T, Ramaswamy S, Ting DT, Lin CP, Toner M, Maheswaran S (2014) Circulating tumor cell clusters are oligoclonal precursors of breast cancer metastasis. Cell 158(5): 1110–1122
4. Steeg PS (2016) Targeting metastasis. Nat Rev Cancer 16(4):201–218
5. Yu M, Bardia A, Aceto N, Bersani F, Madden MW, Donaldson MC, Desai R, Zhu HL, Comaills V, Zheng ZL, Wittner BS, Stojanov P, Brachte E, Sgroi D, Kapur R, Shioda T, Ting DT, Ramaswamy S, Getz G, Iafrate AJ, Benes C, Toner M, Maheswaran S, Haber DA (2014) Ex vivo culture of circulating breast tumor cells for individualized testing of drug susceptibility. Science 345(6193):216–220
6. Mishra A, Dubash TD, Edd JF, Jewett MK, Garre SG, Karabacak NM, Rabe DC, Mutlu BR, Walsh JR, Kapur R, Stott SL,

Maheswaran S, Haber DA, Toner M (2020) Ultrahigh-throughput magnetic sorting of large blood volumes for epitope-agnostic isolation of circulating tumor cells. Proc Natl Acad Sci 117(29): 16839–16847
7. Harouaka RA, Nisic M, Zheng SY (2013) Circulating tumor cell enrichment based on physical properties. J Assoc Lab Autom 18(6): 455–468
8. Jin C, McFaul SM, Duffy SP, Deng X, Tavassoli P, Black PC, Ma H (2014) Technologies for label-free separation of circulating tumor cells: from historical foundations to recent developments. Lab Chip 14(1):32–44
9. Riethdorf S, Fritsche H, Müller V, Rau T, Schindlbeck C, Rack B, Janni W, Coith C, Beck K, Jänicke F, Jackson S, Gornet T, Cristofanilli M, Pantel K (2007) Detection of circulating tumor cells in peripheral blood of patients with metastatic breast cancer: a validation study of the CellSearch system. Clin Cancer Res 13(3):920–928
10. Rawal S, Yang YP, Cote R, Agarwal A (2017) Identification and quantitation of circulating tumor cells. Annu Rev Anal Chem 10: 321–343
11. Zhao WA, Cui CH, Bose S, Guo DG, Shen C, Wong WP, Halvorsen K, Farokhzad OC, Teo GSL, Phillips JA, Dorfman DM, Karnik R, Karp JM (2012) Bioinspired multivalent DNA network for capture and release of cells. Proc Natl Acad Sci 109(48):19626–19631
12. Chen YL, Tyagi D, Lyu MS, Carrier AJ, Nganou C, Youden B, Wang W, Cui SF, Servos M, Oakes K, He SN, Zhang X (2019) Regenerative NanoOctopus based on multivalent-aptamer-functionalized magnetic microparticles for effective cell capture in whole blood. Anal Chem 91(6):4017–4022
13. Wang ZR, Qin WW, Zhuang JL, Wu MH, Li Q, Fan CH, Zhang YQ (2019) Virus-mimicking cell capture using heterovalency magnetic DNA nanoclaws. ACS Appl Mater Interfaces 11(13):12244–12252
14. Song P, Ye DK, Zuo XL, Li J, Wang JB, Liu HJ, Hwang MT, Chao J, Su S, Wang LH, Shi J, Wang LH, Huang W, Lal R, Fan CH (2017) DNA hydrogel with aptamer-toehold-based recognition, cloaking, and decloaking of circulating tumor cells for live cell analysis. Nano Lett 17(9):5193–5198
15. Doane TL, Alam R, Maye MM (2015) Functionalization of quantum rods with oligonucleotides for programmable assembly with DNA origami. Nanoscale 7(7):2883–2888
16. Alexander CM, Hamner KL, Maye MM, Dabrowiak JC (2014) Multifunctional DNA-gold nanoparticles for targeted doxorubicin delivery. Bioconjug Chem 25(7):1261–1271
17. Ding P, Wang Z, Wu Z, Zhu W, Liu L, Sun N (2020) Aptamer-based nanostructured interfaces for the detection and release of circulating tumor cells. J Mater Chem B 8:3408–3422
18. Zheng J, Fang XX, Qin J, Zhang ZF, Miao YM, Yan GQ (2016) A sensitive phosphorescence method based on MPA-capped Mn-doped ZnS quantum dots for the detection of diprophyllin. New J Chem 40(4):3857–3862
19. Reddy SNS, Tan LH, Lu Y (2016) DNA-mediated morphological control of Pd-Au bimetallic nanoparticles. J Am Chem Soc 138(50):16542–16548
20. Chen LH, Liu MC, Tang Y, Chen CF, Wang XX, Hu ZQ (2019) Preparation and properties of a low fouling magnetic nanoparticle and its application to the HPV genotypes assay in whole serum. ACS Appl Mater Interfaces 11(20):18637–18644
21. Panda D, Saha P, Das T, Dash J (2017) Target guided synthesis using DNA nano-templates for selectively assembling a G-quadruplex binding c-MYC inhibitor. Nat Commun 8(1):1–11
22. Chen J, Li CJ, Sun WL, Li YH, Deng CY, Qian H (2019) High catalytic activity of supported au nanoparticles assisted with the surface selective adsorption. J Nanopart Res 21(7):146
23. Miao P, Tang YG, Wang L (2017) DNA modified Fe_3O_4@Au magnetic nanoparticles as selective probes for simultaneous detection of heavy metal ions. ACS Appl Mater Interfaces 9(4):3940–3947
24. Gao T, Wang B, Shi L, Zhu XL, Xiang Y, Anzai JI, Li GX (2017) Ultrasensitive quantitation of plasma membrane proteins via is RTA. Anal Chem 89(20):10776–10782
25. Gao T, Li LL, Chen TS, Shi L, Yang Y, Li GX (2018) DNA-oriented shaping of cell features for the detection of rare disseminated tumor cells. Anal Chem 91(1):1126–1132
26. Gao T, Chen TS, Feng C, He X, Mu CL, Anzai JI, Li GX (2019) Design and fabrication of flexible DNA polymer cocoons to encapsulate live cells. Nat Commun 10(1):1–10
27. Zheng J, Shi H, Wang MJ, Duan CJ, Huang Y, Li C, Xiang Y, Li GX (2019) Homogenous electrochemical method for ultrasensitive detection of tumor cells designed by introduction of poly (A) tails onto cell membranes. Anal Chem 92(2):2194–2200
28. Ke ZF, Lin M, Chen JF, Choi JS, Zhang Y, Fong A, Liang AJ, Chen SF, Li QY, Fang WF, Zhang PS, Garcia MA, Lee T, Song M, Lin HA, Zhao HC, Luo SC, Hou S, Yu HH, Tseng HR (2015) Programming thermoresponsiveness of nanovelcro substrates enables effective purification of circulating tumor cells in lung cancer patients. ACS Nano 9(1):62–70
29. Shen Q, Xu L, Zhao L, Wu D, Fan Y, Zhou Y (2013) Specific capture and release of circulating tumor cells using aptamer-modified nanosubstrates. Adv Mater 25(16):2368–2373
30. Song Y, Shi Y, Huang M, Wang W, Wang Y, Cheng J (2019) Bioinspired engineering of a multivalent aptamer-functionalized nanointerface to enhance the capture and release of circulating tumor cells. Angew Chem Int Ed 131:2258–2262
31. Ding P, Wang Z, Wu Z, Zhou Y, Sun N, Pei R (2020) Natural biointerface based on cancer cell membranes for specific capture and release of circulating tumor cells. ACS Appl Mater Interfaces 12(18):20263–20270
32. Chen JY, Tsai WS, Shao HJ, Wu JC, Lai JM, Lu SH, Hung TF, Yang CT, Wu LC, Chen JS (2016) Sensitive and specific biomimetic lipid coated microfluidics to isolate viable circulating tumor cells and microemboli for cancer detection. PLoS One 11(3):1–21